JACS
JOURNAL OF THE AMERICAN CHEMICAL SOCIETY

COMMUNICATION

pubs.acs.org/JACS

Tissue Morphing Control on Dynamic Gradient Surfaces

Wei Luo and Muhammad N. Yousaf*

Department of Chemistry, University of North Carolina at Chapel Hill, Chapel Hill, North Carolina 27599, United States
Department of Chemistry and Centre for Research on Biomolecular Interactions, York University, Toronto, Ontario M3J 1P3, Canada

Supporting Information

ABSTRACT: In this report, we develop smart surfaces for the spatial and temporal control of mammalian cell behavior. We integrate a bioactive surface strategy with a photo-electroactive surface strategy to generate dynamic ligand surface gradients for controlling cell adhesion, tissue shape morphing, and cell tissue migration.

Mammalian cells exist in a complex and dynamic environment.[1] Cells are continuously bombarded by a myriad of physical-mechanical and hydrodynamic forces along with soluble small molecules and biomolecules.[2] How cells integrate these inputs determines their overall behavior, which ranges from adhesion, migration, and differentiation to apoptosis. For example, during embryonic development the concentration gradients of morphogens determine the position, shape, and size of organs and maps the correct movement of tissue to specific locations.[3] Soluble chemo-attractants direct leukocytes to sites of inflammation, and proper integration of directional cues is essential for proper nerve growth cone guidance.[4] Insoluble gradients derived from the dynamic extracellular matrix (ECM) coordinate cell adhesion and motility for diverse processes from wound healing to metastasis.[5] To address and manipulate dynamic cell behavior, tremendous effort to generate model substrates and 3D scaffolds that can recapitulate these complex processes have been developed. These platforms have been used for cell-based biotechnology assays and tissue engineering and as tools for fundamental studies of cell behavior.[6] One of the most challenging aspects in developing dynamic model substrates is the ability to generate patterned and tailored materials with molecular control of ligand presentation. Herein, we integrate dynamic surfaces with surface gradient technology to generate smart, dynamic molecular gradients for controlled spatial and temporal manipulation of cell tissue movement on surfaces. To our knowledge, until now, there has been no report of dynamic ligand gradients for studies of cell migration or tissue migration.

To generate patterned gradients we used a combined photo- and electroactive surface technology. Previously, we have shown that a photo-protected hydroquinone, upon UV illumination through a microfiche-patterned mask, unveils the hydroquinone group, which can be electrochemically converted to a quinone for subsequent ligand immobilizations with oxyamine-terminated ligands (Figure 1).[7] This strategy allows for the precise generation of ligand patterns and ligand gradient patterns with defined ligand density and slope on a surface. Because all surface molecules are electroactive, this methodology also allows for the quantitative determination of ligand density, since all surface molecules have distinct signatures determined by sensitive cyclic voltammetry techniques.[8] The coupling of oxyamine-terminated ligands and surface-bound quinone is chemoselective and bio-orthogonal and can be done in complex protein mixtures, in cell culture media containing serum, and in the presence of adhered cells to install ligands on the surface. This strategy permits the immobilization of a wide variety of ligands onto a surface for a range of biotechnological microarray applications and cell behavior studies.

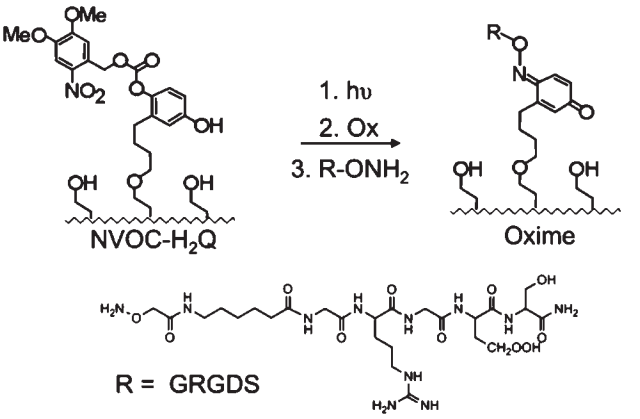

Figure 1. Combined electroactive and photochemical strategy for chemoselective immobilization of ligands in patterns and gradients to a surface. Mixed monolayers presenting photo-protected hydroquinone (NVOC-H_2Q) and tetra(ethylene glycol) groups are illuminated with UV light (365 nm). Photochemical deprotection of the NVOC group reveals the hydroquinone. Electrochemical oxidation converts the hydroquinone to the quinone. The resulting quinone group can then react with oxyamine-tethered peptide ligands (R-ONH_2) to generate stable oxime linkages. The surface-bound molecules are all redox active and therefore allow quantitative determination of the rate of reaction and also the yield of immobilized ligand.

In order to apply this photo-electroactive strategy for dynamic studies of tissue shape morphing and directed tissue migration, we generated surfaces with inert and adhesive regions to cell attachment (Figure 2). We first generated a hydrophobic pattern on a gold substrate by microcontact printing (μCP) hexadecanethiols. The remaining bare gold regions were backfilled with tetra(ethylene glycol)-alkanethiol and NVOC-protected hydroquinone-terminated alkanethiols (98:2 ratio). The high fraction of tetra(ethylene glycol) groups renders the surface inert to nonspecific protein adsorption and cell attachment. Illumination with 365 nm light through a patterned microfiche mask deprotected the NVOC group and revealed the hydroquinone

Received: May 27, 2011
Published: June 27, 2011

dx.doi.org/10.1021/ja204893w | J. Am. Chem. Soc. 2011, 133, 10780–10783

group. The photomask can have a range of geometrical or gradient patterns to generate the corresponding patterns of hydroquinone groups on the surface. The illumination durations and intensity do not compromise the self-assembled monolayer (SAM), and the exposed regions continue to be inert to nonspecific protein adsorption and cell attachment. The unveiled hydroquinone group can be converted to the quinone group by either mild chemical oxidants or a mild oxidative electrochemical applied potential (750 mV for 10 s). In the presence of adhered cells, the quinone group can react rapidly with oxyamine-terminated ligands to form an interfacial chemoselective and bio-orthogonal oxime linkage. This methodology allows for the installation of a range of ligands to a previously inert surface to prepare a variety of tailored surfaces for studies of cell behavior. By using a well-known cell adhesive peptide sequence (RGD peptide), we could generate a dynamic and biospecific surface where different regions of the surface could be converted from nonadhesive to adhesive for cell adhesion. The tripeptide sequence RGD is found in extracellular matrix proteins and has been shown to support cell adhesion and migration by interacting with integrin cell surface receptors.[9]

We demonstrated this strategy by seeding Swiss 3T3 Fibroblast cells to surfaces presenting hydrophobic (hexadecanethiol regions) and photo-deprotected patterned regions presenting hydroquinone groups and tetra(ethylene)glycol groups. Cells adhered only to the μCP hydrophobic regions, where they became confined after they proliferated until becoming contact inhibited. Upon mild oxidative applied potential, the hydroquinone groups were converted to quinone groups. Addition of soluble RGD-oxyamine (5 mM, 20 min) rapidly installed the RGD peptide on the quinone (photo-deprotected) regions. The fibroblast cells on the μCP regions were now able to sense the new adhesive regions and direct their migration outward toward the newly revealed patterned RGD peptides. When a gradient pattern is used, the cells migrate onto the gradient peptides, which can then be used to study directed tissue migration. By varying the ligand, slope, pattern of the gradient, and direction of cell migration (up or down the gradient), many fundamental tissue morphing studies can be performed. By registering the photomask pattern along the μCP regions, controlled and directed cell and tissue migration could be achieved.

Figure 3 shows representative images of cells migrating and morphing on a dynamic substrate from an initial pattern position to a new pattern. Figure 3A shows a μCP hydrophobic circular region surrounded by a tetra(ethylene glycol) and NVOC−hydroquinone SAM. Upon illumination and deprotection through an overlapping square pattern, an inert hydroquinone region is generated (dashed line). Cells attached only to the hydrophobic region and then were allowed to migrate after surface activation and installation of RGD peptides in the square region. Cells immediately migrated and morphed to fill the new pattern. After cell morphing, the cells stayed confined in the new region since the outer regions are still inert to cell attachment and migration. Figure 3B shows a more complex pattern where cells migrated down a gradient and traversed from one pattern to another (circular region to square region) a distance of over 30 μm. Cells are known to extend appendages over 50 μm when migrating. These experiments may be used to study directed cell migration on gradients and the internal cytoskeletal dynamics of lamellipodia and filopodia protrusions from cells during the pattern traversing process.

To investigate how haptotactic gradients affect cell migration, we designed a substrate in which two RGD gradient patterns with

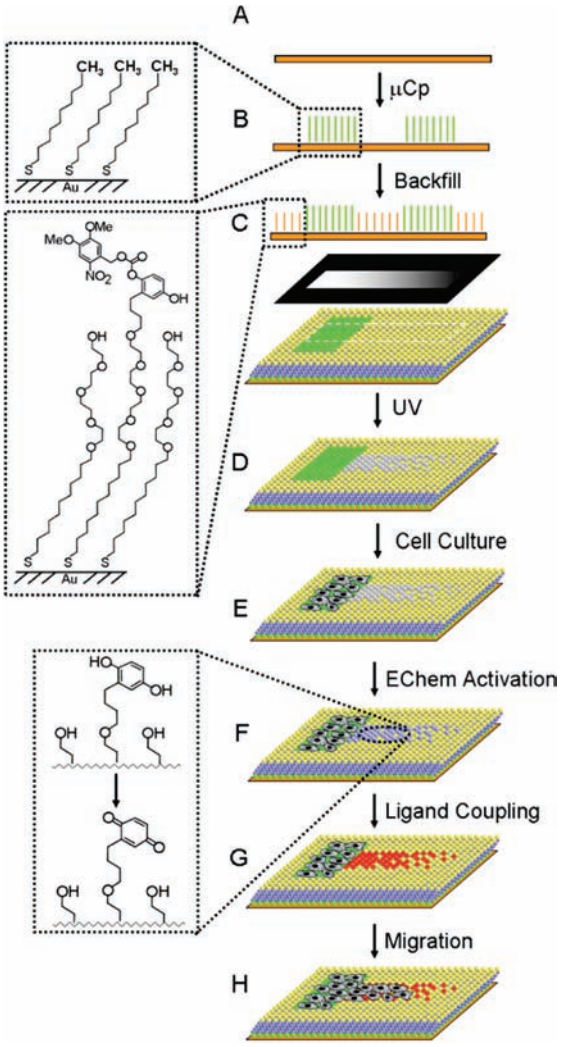

Figure 2. Strategy for the spatial and temporal control of tissue morphing on dynamic patterned and gradient surfaces. (A) An optically transparent gold-coated glass substrate was fabricated by depositing a layer of titanium (5 nm) followed by a layer of gold (10 nm) onto microscope glass coverslips. (B) Hexadecanethiols were microcontact printed in order to generate a hydrophobic pattern on the gold-coated substrate. (C) The remaining bare gold region was backfilled with a mixed monolayer presenting both the NVOC−hydroquinone and tetra(ethylene glycol) groups. (D) UV illumination through a photomask with a gradient pattern deprotected the NVOC groups to reveal the hydroquinone in select regions on the monolayer surface. (E) Fibroblasts were then seeded onto the substrate and adhered exclusively to the hydrophobic patterns. The adherent cells migrated and proliferated until they became contact inhibited but remained confined within the patterns. (F) Application of a mild oxidative potential converted the unreactive hydroquinone monolayer to the corresponding reactive quinone. (G) Addition of soluble adhesive peptide (RGD) oxyamine installed the peptide to the quinone monolayer via a stable oxime formation. The immobilized oxime conjugate modulates the surface property from inert to ligand-mediated cell adhesive. (H) The patterned cells sense the change in the microenvironment and initiate migration outward on the newly defined peptide gradient generated by the photo-patterning.

different slopes were positioned across a μCP line pattern (Figure 4). The substrate was prepared as described in Figure 2 and consisted of a ratio of 98:2 of tetra(ethylene glycol)/alkanethiol:NVOC−H_2Q. Gradients were generated by photo-

dx.doi.org/10.1021/ja204893w |J. Am. Chem. Soc. 2011, 133, 10780–10783

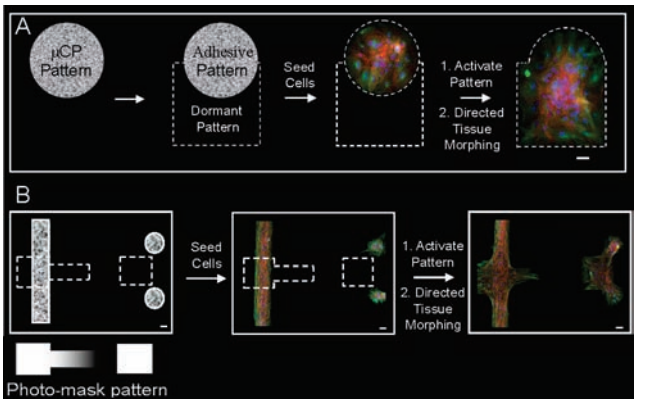

Figure 3. Examples of spatial and temporal control of tissue morphing. Fluorescent micrographs of μCP cells that are able to migrate toward newly unveiled cell-adhesive photopatterned regions. (A) A μCP circular pattern surrounded with an inert mixed NVOC−H_2Q monolayer. Upon illumination through a square photomask, an overlapping square pattern of hydroquinone is unveiled (dashed line). Upon cell seeding, cells attached exclusively to the hydrophobic circular pattern generated by μCP and not to the inert NVOC−H_2Q regions of the surface. Mild electrochemical activation of the surface followed by addition of soluble RGD-ONH_2 resulted in specific immobilization of the peptide to the newly unveiled patterned region. Cells initiated migration and eventually morphed to form a new pattern composed of the μCP region and the RGD-patterned region. Scale bar = 60 μm. (B) Left: A μCP bar and circular pattern surrounded with an inert NVOC−H_2Q monolayer. Upon illumination through an asymmetric dumbbell gradient photomask, an overlapping gradient of hydroquinone is unveiled and a square pattern is seen (dashed lines). Upon cell seeding, cells adhered exclusively to the μCP regions. Surface activation followed by RGD peptide immobilization resulted in cells migrating onto the newly unveiled cell adhesive regions. The gradient region can be monitored to determine cell migration rates up or down gradients. Scale bar = 50 μm.

deprotection of the NVOC−H_2Q group through a patterned gradient microfiche mask followed by RGD ligand immobilization. Time-lapse images of the cells were recorded over 50 h at 37 °C and 5% CO_2. In this experiment, we could test whether the cells tend to migrate up or down the gradient and how fast they migrate according to the underlying gradient of ligands. As shown in the representative micrographs in Figure 4, we defined different zones of migration on the gradient patterns. Uniform density (no gradient) regions were defined as "constant" (green), and cell migration up the gradient was defined as "up" (blue arrow), and cell migration down the gradient was defined as "down" (red). The cells moving in the direction of the red arrows (down) are migrating toward decreasing ligand density (down the gradient). In contrast, cells along the blue arrows are migrating in the direction of increasing ligand density (up the gradient). It is important to note that the slope is the same but the direction of migration of the cells is different (up or down the gradient). The cells initially confined in the μCP lines show active sampling toward RGD patterns by protruding filopodia and lamellipodia. Within 2 h of surface activation and installation of RGD peptides, it was observed that cell fronts started to move onto the RGD gradient patterns. The confluent monolayer of cells on the μCP regions did not lose cell−cell interactions, and the joined cells (tissue) migrate collectively rather than individually. After 40 h cells were found to fill the gradient patterns completely. Since registration of the microfiche mask with the

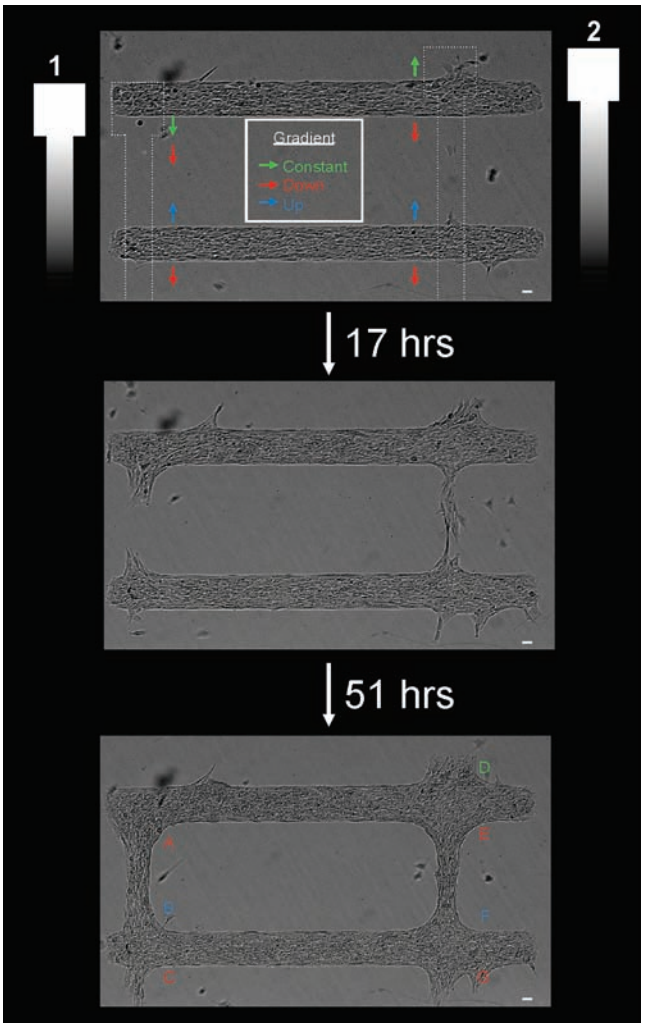

Figure 4. Time-lapse micrographs comparing the migration rates of patterned cells up or down chemoselective RGD peptide gradients. (Top) Two dumbbell-shape gradients of RGD with different slopes were generated across the microcontact printed line patterns of the cells. (Middle) After surface activation and RGD peptide immobilization to the gradient patterns, cells started to migrate from the line patterns and onto the RGD gradient patterns. (Bottom) After 50 h cells completely migrated and filled the gradient regions. Analysis of cell migration rates were compared and depend on the direction of migration on the different slope gradients. The RGD density within the green arrow zone is constant. The cells moving in the direction of the red arrow would be experience decreasing RGD density, while cells migrating in the blue arrow zone are moving up an increasing density of RGD. For further analysis, each zone was labeled as A−G. Scale bar = 100 μm.

μCP regions was straightforward, we were able to repeat this experiment numerous times (n = 44) to obtain statistical data on directional tissue migration rates. The migration of the cell front was measured in each designated region (A−G) and plotted as % migration versus duration to evaluate the rate of tissue migration on the different gradient zones (Figure 5).

From the analysis of several sets of migration data, we found cells on gradient 1 tend to migrate down the gradient (zones A and C) faster than cells migrating up the gradient (zone B). For gradient 2, cells migrated down the gradient (zone E and G) faster than cells migrated up the gradient (zone F). For all experiments the cells migrated the fastest on constant (no

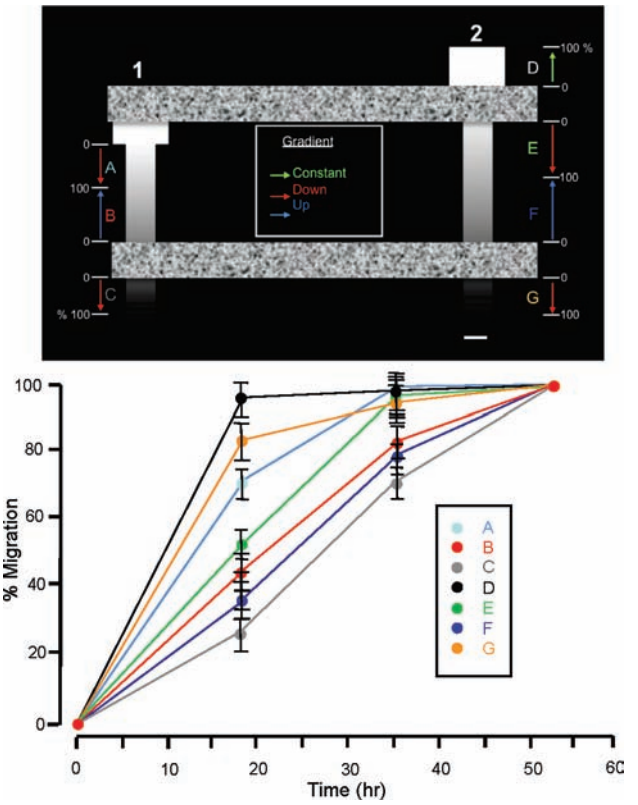

Figure 5. Plot showing migration over time in each zone A−G from Figure 4. (Top) Schematic showing the overlapping gradients and the defined zones of migration on constant, up, or down RGD peptide regions. Each tissue migration zone was set from 0 to 100%, and the % migration was monitored over time in each zone. (Bottom) Plot of % migration versus time for each defined zone. Cells in the high-density RGD zone (D, constant) migrate the fastest. On both gradients (1 and 2) cells migrated faster down the gradient (G, A, E) than up the gradient (B, F). Zone C cells migrated the slowest due to the very low ligand density in this region. Scale bar = 200 μm.

gradient) regions due to the high density of RGD ligands. The slope of gradient 1 is steeper than gradient 2 (Supporting Information), and we observed that cells migrate faster on gradient 1 than gradient 2 (either up or down the gradient). For example, for up the gradient zone B cells migrated faster than zone F, and for down the gradient cells migrated faster in zone A than zone E. For the end of the gradient, which has the lowest ligand density, cells migrated faster on zone G than zone C, most likely due to the very low amount of ligand density to support adhesion and migration in zone C. Overall the cells tend to migrate faster when they move down the gradient rather than up the gradient. Also, the cells on the gradient with steep slope (gradient 1) were observed to respond faster than the cells on the shallow (gradient 2) slope in both directions. As controls, cells did not migrate onto the gradients if the surface was not activated or if a nonadhesive scrambled RDG peptide was installed. Addition of cytoskeleton inhibitors (cytochalasin D and nocodazole (5 mM, 2 h) caused no cell migration on the gradients. Future studies will aim to use different ligands, multiple ligands, multilayers of cells, and co-cultured cells with microfluidic technology to study how cell−cell interactions and cell−material interactions regulate tissue migration.

In summary, we have shown a biospecific and *dynamic gradient* surface for tissue morphing and tissue migration studies. We used an inert SAM surface that presented photo-protected and electroactive molecules that could be activated in the presence of cells for directed tissue migration. We showed the controlled morphing of cells from one pattern to another and that the rate of directed tissue morphing is dependent on the slope and the direction of tissue migration (up or down) on gradients. This dynamic surface strategy may be used as a model substrate to study a range of cell behaviors (adhesion, polarization, migration, differentiation, co-culture paracrine signaling)[10] and as a tumor invasion model system.

■ ASSOCIATED CONTENT

Supporting Information. Experimental details. This material is available free of charge via the Internet at http://pubs.acs.org.

■ AUTHOR INFORMATION

Corresponding Author
mnyousaf@yorku.ca

■ ACKNOWLEDGMENT

This work was supported by the National Science Foundation.

■ REFERENCES

(1) (a) Wong, K.; Park, H. T.; Wu, J. Y.; Rao, Y. *Curr. Opin. Genet. Dev.* **2002**, *12*, 583–591. (b) Schmid, R. S.; Shelton, S.; Stanco, A.; Yokota, Y.; Kreidberg, J. A.; Anton, E. S. *Development* **2004**, *131*, 6023–6031.

(2) (a) Engler, A. J.; Sen, S.; Sweeney, H. L.; Discher, D. E. *Cell* **2006**, *126*, 677–689. (b) Ridley, A. J.; Schwartz, M. A.; Burridge, K.; Firtel, R. A.; Ginsberg, M. H.; Borisy, G.; Parsons, J. T.; Horwitz, A. R. *Science* **2003**, *302*, 1704–1709.

(3) (a) Ashe, H. L.; Briscoe, J. *Development* **2006**, *133*, 385–394. (b) Tabata, T.; Takei, Y. *Development* **2004**, *131*, 703–712. (c) Early, A.; Abe, T.; Williams, J. *Cell* **1995**, *83*, 91–99.

(4) (a) Bar-Shavit, R.; Kahn, A.; Wilner, G. D.; Fenton, J. W. *Science* **1983**, *220*, 728–731. (b) Rosoff, W. J.; Urbach, J. S.; Esrick, M. A.; Mcallister, R. G.; Richards, L. J.; Goodhill, G. J. *Nature Neurosci.* **2004**, *7*, 678–682. (c) Song, H.-j.; Poo, M.-m. *Curr. Opin. Neurobiol.* **1999**, *9*, 355–363. (d) Mueller, B. K. *Annu. Rev. Neurosci.* **1999**, *22*, 351–388.

(5) (a) Lauffenburger, D. A.; Horwitz, A. F. *Cell* **1996**, *84*, 359–369. (b) Aznavoorian, S.; Stracke, M. L.; Krutzsch, H.; Schiffmann, E.; Liotta, L. A. *J. Cell Biol.* **1990**, *110*, 1427–1438. (c) Izaguirre, J. A.; Chaturvedi, R.; Huang, C.; Cickovski, T.; Coffland, J.; Thomas, G.; Forgacs, G.; Alber, M.; Hentschel, G.; Newman, S. A.; Glazier, J. A. *Bioinformatics* **2004**, *20*, 1129–1137.

(6) (a) Liu, B.; Liu, Y.; Riesberg, J. J.; Shen, W. *J. Am. Chem. Soc.* **2010**, *132*, 13630–13632. (b) Robertus, J.; Browne, W. R.; Feringa, B. L. *Chem. Soc. Rev.* **2010**, *39*, 354–378. (c) Jiang, X.; Buzewicz, D. A.; Wong, A. P.; Piel, M.; Whitesides, G. M. *Proc. Natl. Acad. Sci. U.S.A.* **2005**, *102*, 975–978. (d) Shimizu, T.; Yamato, M.; Kikuchi, A.; Okano, T. *Biomaterials* **2003**, *24*, 2309–2316. (e) Yousaf, M. N.; Houseman, B. T.; Mrksich, M. *Proc. Natl. Acad. Sci. U.S.A.* **2001**, *98*, 5992–5996. (f) Nakanishi, J.; Kikuchi, Y.; Inoue, S.; Yamaguchi, K.; Takarada, T.; Maeda, M. *J. Am. Chem. Soc.* **2007**, *129*, 6694–6695. (g) Arnold, M.; Hirschfeld-Warneken, V. C.; Lohmuller, T.; Heil, P.; blummel, J.; Cavalcanti-Adam, E. A.; Lopez-Garcia, M.; Walther, P.; Kessler, H.; Geiger, B.; Spatz, J. P. *Nano Lett.* **2008**, *8*, 2063–2069. (h) Yousaf, M. N.; Lamb, B. M. *ChemBioChem* **2010**, *11*, 745–753.

(7) Chan, E. W. L.; Yousaf, M. N. *Mol. Biosyst.* **2008**, *4*, 746–753.

(8) Luo, W.; Chan, E. W. L.; Yousaf, M. N. *J. Am. Chem. Soc.* **2010**, *132*, 2614–2621.

(9) Huttenlocher, A.; Sandborg, R. R.; Horwitz, A. F. *Curr. Opin. Cell Biol.* **1995**, *7*, 697–706.

(10) Lamb, B. M.; Yousaf, M. N. *J. Am. Chem. Soc.* **2011**, *133*, 8870–8873.